Seismic Discrimination of the May 11, 1998 Indian Nuclear Test with Short-Period Regional Data From Station NIL (Nilore, Pakistan)

Arthur J. Rodgers and William R. Walter

Geophysics and Global Security Division

Lawrence Livermore National Laboratory, Livermore, CA 94551

Correspondence:

Arthur Rodgers, LLNL, L-205, P.O. Box 808, Livermore, CA 94551

Phone (925) 423-5018; fax (925) 423-4077

Email rodgers7@llnl.gov

In preparation for

Pure and Applied Geophysics (PAGEOPH)

Special Volume on Seismic Event Discrimination and Identification

Related to Monitoring a Comprehensive Test Ban Treaty (CTBT)

July 26, 1999

Abstract

Regional seismic discriminants for the May 11, 1998 Indian underground nuclear test(s) and earthquakes recorded at station NIL (Nilore, Pakistan) provide new data to test strategies that can be used to monitor the Comprehensive Nuclear-Test-Ban Treaty (CTBT). Three categories of regional discriminants (ratios of P- and/or S-wave energy) were measured on short-period (0.5-6 Hz) seismograms: P/S amplitude ratios (phase ratios) measured in the same frequency band, P- and S-wave spectral ratios (i.e. low frequency to high frequency for the same phase) and P/S cross-spectral ratios (i.e. low frequency S-wave to high frequency P-wave). The P/S amplitude ratios show good separation of the Indian nuclear test and regional earthquakes for Pn/Lg and Pn/Sn, however Pg/Lg does not discriminate as well. Pn/Lg and Pn/Sn discriminate well at frequencies as low as 0.5-2 Hz, which differs from previous results which report poor separation of earthquakes and explosions at lower frequencies. The P/S amplitude ratios do not show any magnitude dependence, suggesting that forming the ratios in a fixed frequency band cancels the effects of source size-corner frequency scaling. Spatial variability of the observed discriminants arises from variations in crustal waveguide and/or attenuation structure (path propagation effects). Grouping amplitude ratios for earthquakes with paths similar to the Indian test greatly improves discrimination. Removing distance trends does not generally improve discrimination. Accounting for path effects with Bayesian kriging significantly improves discrimination. Spectral ratios (e.g. Pn [0.5-1 Hz]/Pn [4-6 Hz]) and cross-spectral ratios (e.g. Lg [1-2 Hz]/Pn [4-6 Hz]) show distance and magnitude dependence. We developed a technique for simultaneously removing the effects distance and source size-corner frequency scaling. The technique uses a gridsearch to find several parameters that characterize the observed distance and magnitude dependence. Discrimination of the Indian test improved dramatically after the distance and magnitude trends were removed from the spectral and cross-spectral ratio data.

Introduction

The Government of India announced that it detonated three underground nuclear tests on May 11, 1998 at its Pokharan test site in the northwestern Rajasthan desert (Figure 1). The events were routinely located by the United States Geological Survey-Preliminary Determination of Epicenters (USGS-PDE) and by the prototype International Data Center (pIDC). The similarity of teleseismic P-waves of the May 11, 1998 Indian test with the previous 1974 Indian nuclear test suggests that the May 11 test appears seismically as a single large detonation (Wallace, 1998; Barker et al., 1998; Walter et al., 1998). This suggests either near-simultaneous, closely-spaced detonations or one of the tests was much larger than the other two and dominates the waveform. In either case we can treat the May 11 events as a single source. Any complexity that may have arisen from multiple sources is not critical for the purposes of the short-period regional discrimination analysis presented here. This test provides new data for which to investigate regional discrimination strategies in support of Comprehensive Nuclear-Test-Ban Treaty (CTBT) monitoring. In this article we investigate a variety of short-period discriminants using data recorded at station NIL (Nilore, Pakistan).

Many studies have shown that short-period regional discriminants (amplitude or spectral ratios of P- and S-wave energy) are effective at identifying explosions sources (e.g. Taylor et al., 1988, 1989; Walter et al., 1995; Hartse et al., 1997). However, the specific discriminants and frequency bands which best separate explosions from earthquake populations vary from region to region due to near source and along-path propagation effects. Thus, one of the challenges of CTBT monitoring at regional distances is to determine which are the best discriminants in a given region. This is difficult to do globally because nuclear tests have been performed in only a few places since the current network of global broadband seismic stations has been operational. The May 11 event was well recorded at regional distance by station NIL (Nilore, Pakistan; see Figure 1). Figure 2 shows the NIL recording of the Indian test. This event had a body-wave magnitude, m_b, of 5.2 and a surface wave magnitude, M_S, of 3.5 as reported in the USGS-PDE. Although this event was large

enough to be identified as an explosion by the teleseismic M_S:m_b discriminant, nuclear tests smaller than m_b 4.5 in the future may not be discriminated teleseismically due to poor signal-to-noise at distances greater than 2000 km. In this paper, we show that short-period (0.5-6 Hz) regional discriminants (P/S amplitude ratios, phase-spectral ratios and cross-spectral ratios) measured at NIL clearly identify the May 11 Test as an explosion. We also show that procedures which account for distance effects, laterally variable path effects and source size effects can dramatically improve discrimination.

Regional Events and Discriminant Measurements

Waveform data for earthquakes recorded at station NIL were selected from our research database (Ruppert et al., 1998). Event locations and origin times were taken from the USGS-PDE. We selected events with reported depths less than 50 km. Distances were limited to 200-1500 km to avoid problems with Pg-Pn interference at close distances and upper mantle triplication body-waves at far-regional distances. The earthquake and Indian test locations are shown in Figure 1. All waveforms were previewed and data with glitches and/or poor signal-to-noise were discarded. The first arriving P-wave was picked on vertical components. In this study only vertical component waveforms were used. The SHZ and BHZ channels at NIL recorded broadband velocities at 40 samples/second and 20 samples/second, respectively. The instrument response was removed and the amplitude spectra were recorded as the Fourier transform of ground displacement. The NIL amplitude ratios were taken from the SHZ channel. Additional 39 events were recorded on the BHZ channel that were not available on the SHZ channel. In order to provide the most complete data set for station NIL, we merged the amplitude measurements for both SHZ and BHZ together for this study. For frequencies below the anti-aliasing filter of the BHZ channel (~6.0 Hz) the spectra of any phase for a given event are identical. Thus we limited the maximum frequency of amplitude and spectral ratios to 6.0 Hz.

Regional phases were isolated with the following group velocity windows: Pn 8.25-7.7 km/s; Pg 6.5-5.5 km/s; Sn 4.6-4.0 km/s and Lg 3.6-3.0 km/s. The phase windows were uniformly shifted so that the P-wave arrives at 8.25 km/s plus static delay time of 10.0 s, nominal Pn velocity and crustal leg times for the region. This time shift accounts for small errors in the location, origin time and station clock accuracy and ensures that the regional phases are windowed uniformly. We discarded traces for which this shift was greater than ±10 seconds, as these events have more significant timing and/or location problems. Amplitudes were measured in four frequency bands (0.5-1.0, 1.0-2.0, 2.0-4.0, and 4.0-6.0 Hz) from the smoothed amplitude spectrum of each phase, as in previous studies (e.g. Rodgers et al., 1999). Noise measurements were made on 30 second pre-Pn windows. Figure 2 illustrates the windows used to isolate the phases and noise for the Indian test and a nearby earthquake.

Discriminants were formed from the amplitude measurements. We used only amplitudes that had a signal-to-noise ratio greater than 5:1 within a given frequency band. Three classes of short-period discriminants were formed from the observed amplitudes: P/S amplitude or phase ratios (e.g. Pn/Sn, Pn/Lg and Pg/Lg in the same frequency band); spectral ratios (low frequency to high frequency ratios of the same phase such as Pn[0.5-1 Hz]/ Pn[4-6 Hz]); and cross-spectral ratios (low frequency S to high frequency P ratios such as Lg[1-2 Hz]/Pn[4-6 Hz]). The distance and magnitude dependence of each discriminant was investigated along with its spatial variability. Figure 3a and 3b shows the magnitude and distance dependence for one of each class of discriminant, respectively. A linear regression on distance was computed using the earthquake data (shown in Figure 3b). This trend was removed from both the earthquake and explosion data and the resulting magnitude dependence is shown in Figure 3c. These plots show that two of the three discriminants have a strong distance dependence and that discriminants involving a spectral ratio have a magnitude dependence, especially the Lg[1-2 Hz]/Pn[4-6 Hz] discriminant. This magnitude trend results from source size-corner frequency scaling. Correction of this source size-corner frequency scaling effect will be discussed below.

P/S Amplitude Ratios

The Pn/Lg [1-2 Hz] amplitude ratios shown in Figure 3 show that the Indian Test has on average a higher P/S ratio than the earthquakes recorded at station NIL. This is consistent with the absence of S-wave energy (Lg) from the explosion source, whereas the earthquakes have larger S-wave amplitudes (lower Pn/Lg ratios). The Pn/Lg [1-2 Hz] amplitude ratios plotted in Figure 3a and 3c show no magnitude dependence. We found this to be true for other P/S ratios and frequency bands. This indicates that any source size-corner frequency scaling affects both P- and S-waves identically, or that any source size effect is smaller than the scatter that arises from propagation path effects and/or source depth or radiation pattern effects. There is a strong distance dependence for the Pn/Lg [1-2 Hz] amplitude ratios seen in Figure 3b (left). Removing this distance trend reduces the scatter of the earthquake population but does not necessarily improve the separation of the Pn/Lg [1-2 Hz] discriminant for the Indian test and the earthquakes. The remaining scatter in the earthquake population is due to path effects and/or source depth and radiation effects. In order to visualize these propagation path effects, we map the observed amplitude ratios projected to their event locations in Figure 4. The ratios in Figure 4 show that events to the north tend to have higher ratios (weaker Lg energy relative to Pn) than those from the south, however it is important to note that these data were not corrected for their distance trend.

Large variations in topography (Figure 1), crustal thickness and attenuation structure may weaken Lg amplitudes for the northern paths relative to those from the south (see for example Fan and Lay, 1998). Thus, it may be wise to compare the Indian nuclear test with earthquakes having similar paths to NIL. Limiting back-azimuths to isolate events having similar paths resulted in better representations of the distance trends for earthquake ratios observed at station ABKT

(Rodgers et al. 1999). In Figure 4 we show azimuthal rays at 100° and 255° which isolate the southerly events with paths restricted more or less to the Indian Platform. In Figure 5 we show the Pn/Lg, Pg/Lg and Pn/Sn amplitude ratios of the Indian test and the southerly earthquakes for several frequency bands. When only events from the southerly back-azimuths are considered, the Pn/Lg and Pn/Sn ratios above 2 Hz clearly separate the Indian test from the earthquakes. However, the Pg/Lg ratios do not discriminate as well as the ratios involving Pn. Pg amplitudes are less scattered than Pn amplitudes probably because Pg is composed of multiply reflected waves, which sample a large part of the focal sphere. It is remarkable that the lower frequency Pn/Lg and Pn/Sn ratios (0.5-2 Hz) discriminate almost as well as higher frequency ratios. It is usually the case that discrimination performance improves as frequency increases, especially for frequencies above 3.0 Hz (e.g. Walter et al., 1995; Hartse et al., 1997).

To further illustrate the importance of path effects on discrimination, we show the Mahalanobis distance as a function of frequency band for all azimuths and for just the southerly events (Figure 6). The Mahalanobis distance, D^2, is a measure of the separation of two populations. It is computed using the following equation:

$$D^2 = (\mu_{ex} - \mu_{eq})^2 / (\sigma^2_{ex} + \sigma^2_{eq}) ;$$

where μ and σ^2 are the mean and variance, respectively, for the explosion (ex) and earthquake (eq) populations. We assume the Indian test represents the mean of the (unknown) explosion population and that the variance of the explosion population is equal to that of the earthquakes for each ratio. Using the one test as the mean is the simplest assumption we can make, while using the earthquake variance is probably conservative. Despite the uncertainty of these assumptions, using equation (1) provides a simple objective measure to compare the separation of each of the various discriminants for the earthquakes and the Indian test. Figure 6 shows that the Mahalanobis

distance is much greater when the Indian test ratios is compared with earthquakes from the south of NIL, emphasizing the importance of path effects. We found that when the distance trends were removed there was little change in the Mahalanobis distance regardless of how the data were grouped.

The path variability seen in the map of Pn/Lg ratios (Figure 4) can be represented by a correction surface generated with Bayesian kriging (Schultz et al., 1998). This technique has been shown to be superior to other strategies for representing regional P/S ratios because it provides a smooth, continuous correction surface with uncertainty estimates and results in the best representation of the data (Rodgers et al., 1999). Figure 7 shows a map of the distance corrected Pn/Lg [1-2 Hz] ratios plotted on top of the correction surface obtained from the kriging algorithm. Notice that the surface predicts low Pn/Lg ratios (< 0.0) near the Indian test site, corresponding to strong Lg energy relative to Pn. Applying the corrections predicted by the kriged surface results in improved discrimination. Figure 8 shows the Pn/Lg [1-2 Hz] for all azimuths as a function of magnitude without any correction, with distance corrections and with the distance and path corrections from kriging. Note that the separation of the Indian test from the mean of the earthquakes is greater in Figure 8c than in Figure 8a and 8b and that the scatter (rms) of the earthquake population is reduced significantly after the path corrections were applied. Reducing the scatter and separating the means of the earthquake and explosion populations is necessary for good discrimination.

Spectral and Cross-Spectral Ratios

The distance corrected spectral and cross-spectral ratios shown in Figure 3c discriminate the Indian test from events of about the same magnitude. However, this is not the case when the Indian

test is compared to events of smaller magnitude. For models of earthquake or explosion generated seismic phase spectra, forming the ratio of amplitudes in two different frequency bands leads to a magnitude dependence (Taylor and Denny, 1991; Walter and Priestley, 1991, Taylor et al., 1998). This arises because the corner frequency of the source amplitude spectrum is inversely proportional to the seismic moment. The magnitude dependence of spectral ratios (e.g. Pn [0.5-1 Hz]/Pn [4-6 Hz]) and cross-spectral ratios (e.g. Lg [1-2 Hz]/Pn [4-6 Hz]) leads to two undesirable consequences. Firstly, there is excess scatter, which may inhibit discrimination performance when events of different sizes are compared. Secondly, and more importantly, the spectral ratio discriminants are not normally distributed and thus fail a basic assumption necessary for multivariate discrimination strategies. The magnitude dependence can be removed if a model of the source size-corner frequency scaling is obtained.

Recently, Taylor and Hartse (1998) described a procedure for modeling absolute amplitude spectra of regional phases (the source path amplitude correction or SPAC method). They based their method on a model of regional phase amplitudes that depends on the seismic moment (low-frequency spectral level), a Brune (1970) earthquake source model, a source size-corner frequency scaling relation, geometric spreading and frequency-dependent attenuation. An iterative inversion algorithm fits all observed spectra of a given phase to several model parameters. Because of severe trade-off between some model parameters (especially geometric spreading and attenuation), some model parameters are fixed while the remaining parameters are estimated by inversion and checked to see if they are physically reasonable.

We developed a grid-search method to correct regional spectral and cross-spectral ratios for the combined dependence on distance (through geometric spreading and attenuation) and magnitude (through source size-corner frequency scaling) such as that seen in Figure 3. The theory is described in detail in the Appendix. The method is based on the same theory of regional

phase amplitude spectra that is used by SPAC (Taylor and Hartse, 1998). However, we chose to model the distance and magnitude (log seismic moment) dependence of the discriminant ratios, rather than model the absolute amplitude behavior of the individual phases. In this way we explicitly link the source parameters for each phase in the cross-spectral ratios, rather than fit phases independently as in the SPAC method (Taylor and Hartse, 1998). Our hope was that by dealing with only the relative source and path terms in ratios we could better bound the source-path tradeoffs. Currently we are working with Taylor and others to combine the best aspects of both the SPAC technique and that described here. The results of those efforts will be described in a future paper.

Given the model of regional phase amplitude spectra, the 10-base log of a cross-spectral ratio of an S-wave at frequency f_1, $S(f_1)$, and P-wave at frequency f_2, $P(f_2)$, can be expressed as:

$$Log10\ [\ S(f_1) / P(f_2)\ ] = C + f(f_1, f_2, F, a, \kappa; M_0) + G\ log_{10}\ \Delta + D\ \Delta \quad ; \qquad (1)$$

where C is a constant, F is the source moment-corner frequency scaling parameter, a is the P-wave to S-wave corner frequency scaling parameter, κ is the source moment-corner frequency scaling exponent, M_0 is the seismic moment, G is the $\log_{10}$ distance parameter (related to geometric spreading), Δ is the distance and D is the linear distance parameter (related to attenuation). The function $f\ (f_1, f_2, F, a, \kappa; M_0)$ describes the variation of the spectral ratio with source size (moment), and is plotted in the Appendix (Figure A1b). The PDE body-wave magnitudes for the events considered were converted to seismic moments using the scaling relation from Cong et al. (1996): $log_{10}\ M_0 = 10.66 + 1.04\ mb$. We found with several data sets, including both amplitude and spectral ratios, that the $log_{10}\ \Delta$ term is not well resolved when both linear and log distance terms are sought. Therefore we only consider the linear distance term in our parameter search (G=0). For spectral ratios, the $log_{10}\ \Delta$ term and the P-wave to S-wave corner frequency scaling constant, a, drop out. To constrain the search, we chose to fix the source moment corner frequency scaling exponent,

κ = 1/3, and the P-wave to S-wave corner frequency scaling constant, a = 1.7 (for cross-spectral ratios only). We searched over ranges of C, D and F and minimized the error. Error was measured as the data normalized sum of the squared residuals between the observed spectral ratios and the model predictions. Best-fitting parameters are those that provide the minimum error (misfit). Many experiments were run to ensure that the ranges and increments of parameter values for the grid-search were sufficient to resolve the best-fitting values. Grid-searches run with κ = 1/4 and/or a = 1.0 resulted in a similar fit to the spectral ratio data.

Figure 9 shows the contoured error surfaces for the Lg [1-2 Hz] / Pn [4-6 Hz] spectral ratios. The model uncertainties and trade-off between parameters can be inferred from these plots. Note that the moment scaling constant, F, is poorly resolved and trades-off to some extent with the constant term, C, and the distance term, D. The distance term, D, obtained from the grid-search (-0.001 km^{-1}, is similar to the value obtained from linear regression on distance alone (-0.0008 km^{-1}), which suggests that the distance and magnitude dependence are more or less independent. The fact that the moment scaling constant, F, is poorly resolved is not surprising given that the function $f(f_1, f_2, F, a, \kappa; M_0)$ is only weakly dependent on this parameter. Viewing the model predictions plotted over the data can see the performance of this technique. Figure 10 shows the moment corrected Lg [1-2 Hz] / Pn [4-6 Hz] spectral ratios as a function of distance and the distance corrected spectral ratios as a function of moment, along with the best-fitting model predictions. The variance of the earthquake population is reduced by 33% by the joint distance and moment modeling, compared to a variance reduction of 18% for the (linear) distance dependence alone. The resulting distance and moment dependence after the model predictions were applied, shown in Figure 11, indicates that the distance and moment trends are removed by our method. The spectral ratio for the Indian test was corrected by the same model and is also shown in Figure 11. The discrimination of the test is better for the corrected data than the uncorrected data (compare with Figure 3a).

Discussion

The May 11, 1998 Indian nuclear test provides valuable new data to calibrate regional discrimination strategies in support of Comprehensive Nuclear-Test-Ban Treaty (CTBT) monitoring. The Indian test is well discriminated from regional earthquakes observed at station NIL (Nilore, Pakistan). The test shows high values for P/S ratios and small values for low-frequency/high-frequency spectral ratios, consistent with an explosion source. Particularly remarkable is that even relatively low frequency (< 3 Hz) P/S ratios, especially Pn/Sn and Pn/Lg, show good separation between the regional earthquakes and the test and the results do not improve as one moves to higher frequencies. This is quite different from discrimination results in a number of previous studies in other areas of the world, which show P/S discrimination is poor-to-fair and lower frequencies (0.5-4 Hz) and improves as one moves to higher frequencies. Examples include the U.S. Nevada Test Site (e.g. Walter et al., 1995), the Former Soviet Union Semipalitinsk test site in Kazakhstan and the Lop Nor test site in China (e.g. Hartse et al.1997). Similar results have been found in studies discriminating mining explosions from earthquakes in Scandinavia (e.g. Baumgardt and Young, 1990), the eastern U.S. (e.g. Kim et al. 1993) and the Caucasus (e.g. Kim et al 1997). The discrimination of the Indian test and regional earthquakes using P/S ratios as shown in Figure 5 do not show this frequency dependence, in fact discrimination appears slightly better in the lower frequencies than above 4 Hz.

The propagation of S-wave phases is efficient and attenuation is probably low for the paths through the Indian Platform to the south of NIL (Ni and Barazangi, 1983). We believe the S-waves from the earthquakes south of NIL are clearly observed and the propagation effects properly accounted for. However, the source of explosion S-waves from the Indian test, and explosions in general, has been the source of numerous investigations over the years and remains an area of active research. One possible source of shallow explosion S-waves in the .5-4 Hz frequency band is from Rg-to-S scattering (e.g. Gupta et al. 1992; Patton and Taylor, 1995; Mayeda and Walter, 1996). Myers et al. (1999) have recently examined the 1997 Kazakhstan depth-of-burial experiment and

find strong evidence to support this idea. In particular Myers et al. (1999) observe strong Rg decay in the 0.7 to 5 Hz frequency band within 20 km of the explosions. They note the regional S-waves and S-wave coda show increases in amplitude in this same band, as the shot depth shallows, consistent with an Rg scattering as the source for the observed explosion S-waves. One possibility is that in the relatively flat lying terrain and geology of the Indian Test site such Rg-to-S scattering is much less efficient that at other test sites such as NTS, Lop Nor and Semipalitinsk.

This paper demonstrates that proper calibration of distance and path effects is very important to effective regional discrimination. The trends shown in Figure 3b indicate that distance effects can be significant. Removing the distance trends by regression reduces the scatter in the earthquake population. Path effects on discriminants arise from lateral variations in elastic and anelastic structure associated with tectonic features. Kriging has been shown to be the best method to account for path effects on discriminants (Rodgers et al, 1999, Phillips, 1999). We show that applying the path corrections predicted from kriging improves the separation of the Indian test and regional earthquakes (Figure 8).

Spectral ratios have a magnitude dependence that results from source size-corner frequency scaling. We show that magnitude and distance trends of spectral ratios can be simultaneously removed. Our method is based on a simple theoretical model of regional phase amplitudes, a Brune earthquake source model and source size-corner frequency scaling relationship (Appendix). The method uses a grid-search to estimate three parameters that control the magnitude and distance trends. Removing the magnitude and distance trends of spectral ratios improves the separation of regional earthquakes and the Indian test. More importantly, the resulting corrected spectral ratios are more normally distributed, which is essential for multivariate discrimination algorithms such as linear discriminant analysis (LDA). The corrected spectral ratios have no appreciable magnitude or distance dependence (Figure 11). A drawback of our method is that the earthquake data often span

a limited magnitude range (m_b 4.0-6.0, e.g. Figure 3c). Small events ($m_b < 4.0$) will be of particular interest to CTBT monitoring. The ability of our correction procedure to account for the magnitude dependence of these small events will depend critically on having a training set of small magnitude earthquakes. In regions with very few earthquakes and/or limited magnitude ranges of data the correction procedure will have to rely heavily on expert knowledge to properly extrapolate from the fits of limited data to the magnitudes, distances and locations of interest. In this regard having a good understanding of both the source scaling and the underlying attenuation in the region will be important. Other types of structural or hazard investigations (attenuation tomography, refraction line interpretations, stress drop studies, etc.), provide some information on these topics in regions where seismicity is limited. Because the method outlined here uses simple theoretic formulations for source scaling, geometrical spreading and attenuation, it is easy and straightforward to incorporate and evaluate such results from other studies.

In this paper, we showed that the May 11, 1998 Indian nuclear test could be clearly identified as an explosion using regional discrimination techniques developed in other areas of the world (e.g. western U.S., Kazakhstan, China). This result shows the strength of regional discrimination techniques and the value of regional distance data for CTBT monitoring down to fairly small magnitudes. These results also give us some confidence that regional discriminants developed at former test sites can be transported to other areas of the world if the proper path and source calibrations are done. This is important since in many regions of the world regional CTBT monitoring will need to be done without any empirical nuclear explosion calibration data.

Acknowledgments

Waveform data was obtained from the Incorporated Research Institutions for Seismology - Data Management Center (IRIS-DMC). Waveform data was collected and organized by Stan

Ruppert, Terri Hauk and Jennifer O'Boyle. Research was performed under the auspices of the U.S. Department of Energy by the Lawrence Livermore National Laboratory under contract W-7405-ENG-48. This is LLNL journal contribution UCRL-JC-134453.

References

Barker, B. and 18 others (1998). Monitoring Nuclear Tests, *Science*, 281.

Baumgardt, D. R. and G. B. Young (1990), Regional seismic waveform discriminants and case based event identification using regional arrays, *Bull. Seism. Soc. Am., 80*, 1874-1892.

Brune, J. (1970). Tectonic stress and the spectra from seismic shear waves earthquakes, *J. Geophys. Res.*, **75**, 4997-5009.

Cong, L., J. Xie and B. Mitchell (1996). Excitation and propagation of Lg from earthquakes in Central Asia with implications for explosion/earthquake discrimination, *J. Geophys. Res.*, **101**, 27,779-27789.

Fan, G. and T. Lay (1998c). Regionalized versus single-station waveguide effects on seismic discriminants in western China, *Bull. Seism. Soc. Am.*, **88**, 1260-1274.

Gupta, I. N., W. W. Chan, and R. A. Wagner (1992). A comparison of regional phases from underground nuclear explosions at East Kazakh and Nevada Test Sites, *Bull Seism. Soc. Am.* **82**, 352-382.

Hartse, H., S. Taylor, S. Phillips and G. Randall (1997). A preliminary study of regional seismic discrimination in Central Asia with emphasis on western China, *Bull. Seism. Soc. Am.* **87**, 551-568.

Kim, W. –Y., D. Simpson, and P. Richards (1993). Discrimination of earthquakes and explosions in the eastern United States using regional high-frequency data, *Geophys. Res. Lett.*, **20**, 1507-1510.

Kim, W. –Y., V. Aharonian, A. L. Lerner-Lam, and P. G. Richards (1997), Discrimination of earthquakes and explosions in Southern Russia using regional high-frequency three-

component data from the IRIS/JSP Caucasus network, Bull. Seism. Soc. Am., 87, 569-588.

Mayeda, K., and W. Walter (1996). Moment, energy, stress drop and source spectra of western United States earthquakes from regional coda envelopes, *J. Geophys. Res.* **101**, 11,195-11,208.

Myers, S. C., W. R. Walter, K. Mayeda and L. Glenn (1999), Observations in support of Rg scattering as a source of explosion S waves: regional and local recordings of the 1997 Kazakhstan depth of burial experiment, *Bull. Seism. Soc. Am.*, **89**, 544-549.

Ni, J. and M. Barazangi (1983). High-frequency seismic wave propagation beneath the Indian Shield, Himalayan Arc, Tibetan Plateau and surrounding regions: high uppermost mantle velocities and efficient propagation beneath Tibet, *Geophys. J. R. astr. Soc.*, **72**, 665-689.

Patton, H. J. and S. R. Taylor, (1995). Analysis of Lg spectral ratios from NTS explosions: implications for the source mechanisms of spall and the generation of Lg waves, *Bull. Seism. Soc. Am.*, **85**, 220-236.

Rodgers, A., W. Walter, C. Schultz, S. Myers and T. Lay (1999). A comparison of methodologies for representing path effects on regional P/S discriminants, *Bull. Seismo. Soc. Amer.*, **89**, 394-408.

Ruppert, S., T. Hauk, R. Leach and J. O'Boyle (1998). LLNL Middle East and North Africa Research Database, *Proceedings of the 20th Annual Seismic Research Symposium on Monitoring a Comprehensive Test Ban Treaty*, Santa Fe, NM, Department of Defense, Nuclear Treaty Programs Report, 727-735.

Taylor, S., N. Sherman and M. Denny (1988). Spectral discrimination between NTS explosions and western United States earthquakes at regional distances, *Bull. Seism. Soc. Am.*, **78**, 1563-1579.

Taylor, S., M. Denny, E. Vergino and R. Glaser (1989). Regional discrimination between NTS explosions and western U.S. earthquakes, *Bull. Seism. Soc. Am.*, **79**, 1142-1176.

Taylor, S. and M. Denny (1991). An analysis of spectral differences between NTS and Shagan River nuclear explosions, *J. Geophys. Res.*, **96**, 6237-6245.

Taylor, S. and H. Hartse (1998). A procedure for estimation of source and propagation corrections for regional seismic discriminants, *J. Geophys. Res.*, **103**, 2781-2789.

Schultz, C, S. Myers, J. Hipp and C. Young (1998). Nonstationary Bayesian kriging: application of spatial corrections to improve seismic detection, location and identification, *Bull. Seism. Soc. Am.*, **88**, 1275-1288.

Wallace, T. (1998).The May 1998 Indian and Pakistan Nuclear Tests, *Seismo. Res. Lett.*, **69**, 386-393.

Walter, W., and K. Priestley (1991). High-frequency P wave spectra from explosions and earthquakes, in *Explosion Source Phenomenology*, ed. S. Taylor, H. Patton and P. Richards.

Walter, W., K. Mayeda and H. Patton (1995). Phase and spectral ratio discrimination between NTS earthquakes and explosions. Part I: empirical observations, *Bull. Seism. Soc. Am.*, **85**, 1050-1067.

Walter, W., A. Rodgers, K. Mayeda, S. Myers, M. Pasyanos and M. Denny (1998). Preliminary regional seismic analysis of nuclear explosions and earthquakes in southwest Asia, *Proceedings of the 20th Annual Seismic Research Symposium on Monitoring a Comprehensive Test Ban Treaty*, Santa Fe, NM, 23-25 September, 1998, Department of Defense, Nuclear Treaty Programs Report, 387-396.

Figure Captions

Figure 1. Map of station NIL (green triangle), the Indian test (red diamond) and regional earthquakes (blue circles) used in this study. The waveform shown in Figure 2 is for the earthquake marked 95094.

Figure 2. NIL vertical component recordings of the Indian test (top) and a nearby 95094 earthquake (bottom, location shown in Figure 1). Both traces were bandpass filtered 0.5-6 Hz. Vertical lines indicate phase and noise windows.

Figure 3. (a) Magnitude dependence, (b) distance dependence and (c) distance-corrected magnitude dependence for three classes of discriminants for the earthquakes (circles) and the Indian test (diamond) recorded at NIL. The discriminants shown are Pn/Lg [1-2 Hz] (left column); Pn [0.5-1 Hz]/ Pn [4-6 Hz] (center column); and Lg [1-2 Hz]/ Pn [4-6 Hz] (right column).

Figure 4. Map of Pn/Lg [1-2 Hz] amplitude ratios for the regional earthquakes (circles) and the May 11 Indian test (diamond). Rays drawn from station NIL indicate the back-azimuthal limits used to isolate events from the south.

Figure 5. Distance corrected amplitude ratios plotted at the center frequency for Pn/Lg (top); Pg/Lg (middle) and Pn/Sn (bottom). Only events from southerly back-azimuths (90°-255°) from NIL are shown.

Figure 6. Mahalanobis distance (see text) as a function of frequency band for all azimuths (circles) and the southerly azimuths (triangles).

Figure 7. Distance corrected Pn/Lg [1-2 Hz] ratios plotted over the correction surface obtained from kriging. Also shown is the distance corrected Pn/Lg ratio of the Indian test.

Figure 8. Pn/Lg [1-2 Hz] versus PDE mb for all azimuths only: (a) uncorrected ratios; (b) ratios corrected for the distance trend and (c) ratios corrected with the kriged correction surface. Circles indicate earthquakes and the diamond indicates the Indian test. Also shown are the mean and standard deviation (rms) of the earthquake population in each case.

Figure 9. Slices through the model error (misfit) surfaces: (a) D vs. C; (b) F vs. C; and (c) F vs. D. Each surface is plotted with the third parameter held at its best-fitting value. Best-fitting parameters are indicated by black dots at the minimum misfit.

Figure 10. Lg [1-2 Hz] / Pn [4-6 Hz] spectral ratios (a) corrected for the moment scaling and plotted versus distance and (b) corrected for the distance dependence and plotted versus log moment. The model predictions are plotted as the dashed lines.

Figure 11. The Lg [1-2 Hz] / Pn [4-6 Hz] spectral ratios corrected for the best-fitting model and plotted versus (a) distance and (b) moment. The earthquakes are indicated as blue circles and the red diamond indicates the Indian test. Linear regressions and 1-σ uncertainties are also plotted, showing that the distance and log moment dependence is removed after correction. The linear correlation (lincorr) and slope of the regression line for each case are also shown.

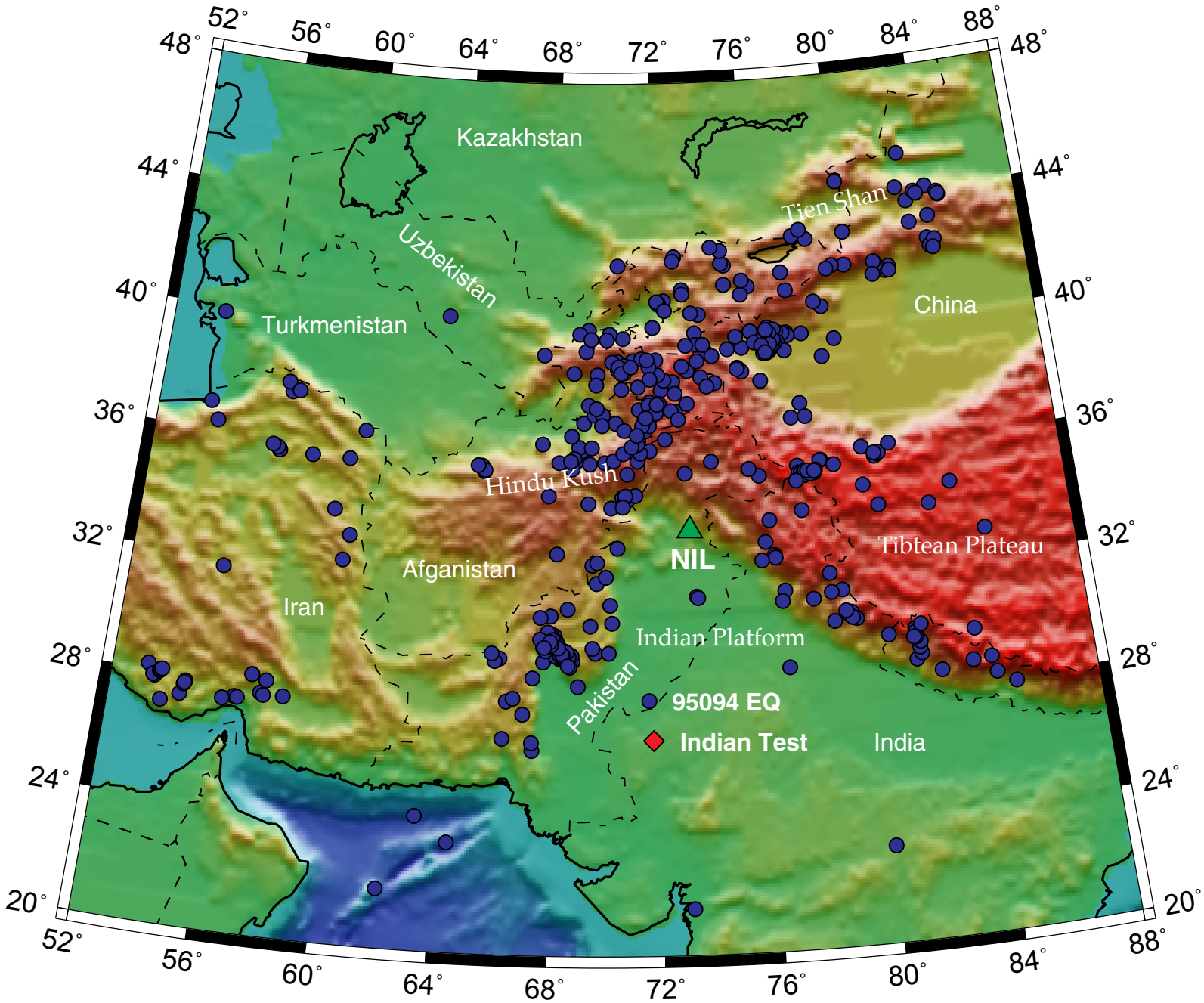

Rodgers and Walter, Regional Discrimination of Indian Test, 1999, Figure 1

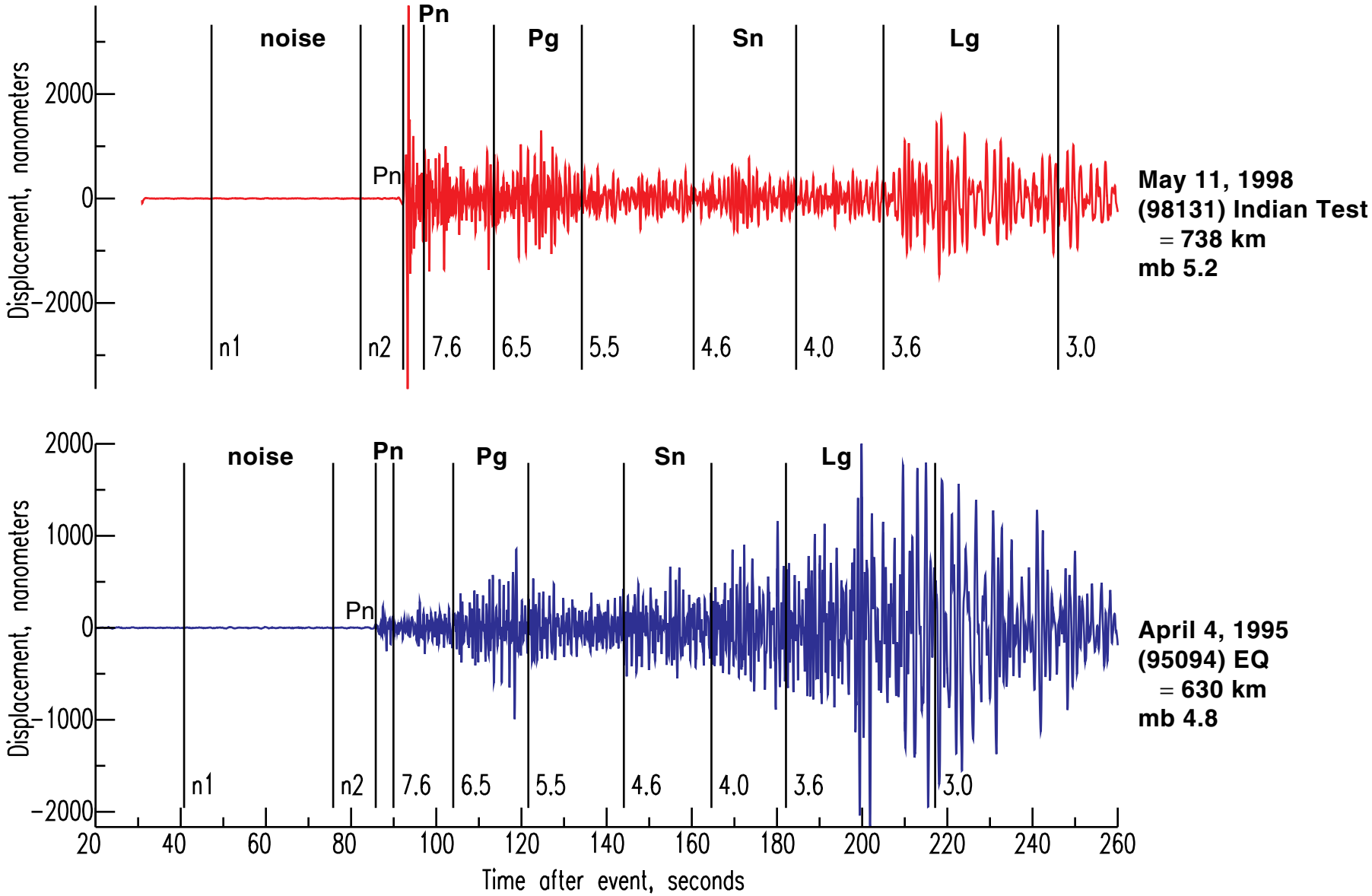

Rodgers and Walter, Regional Discrimination of Indian Test, 1999, Figure 2

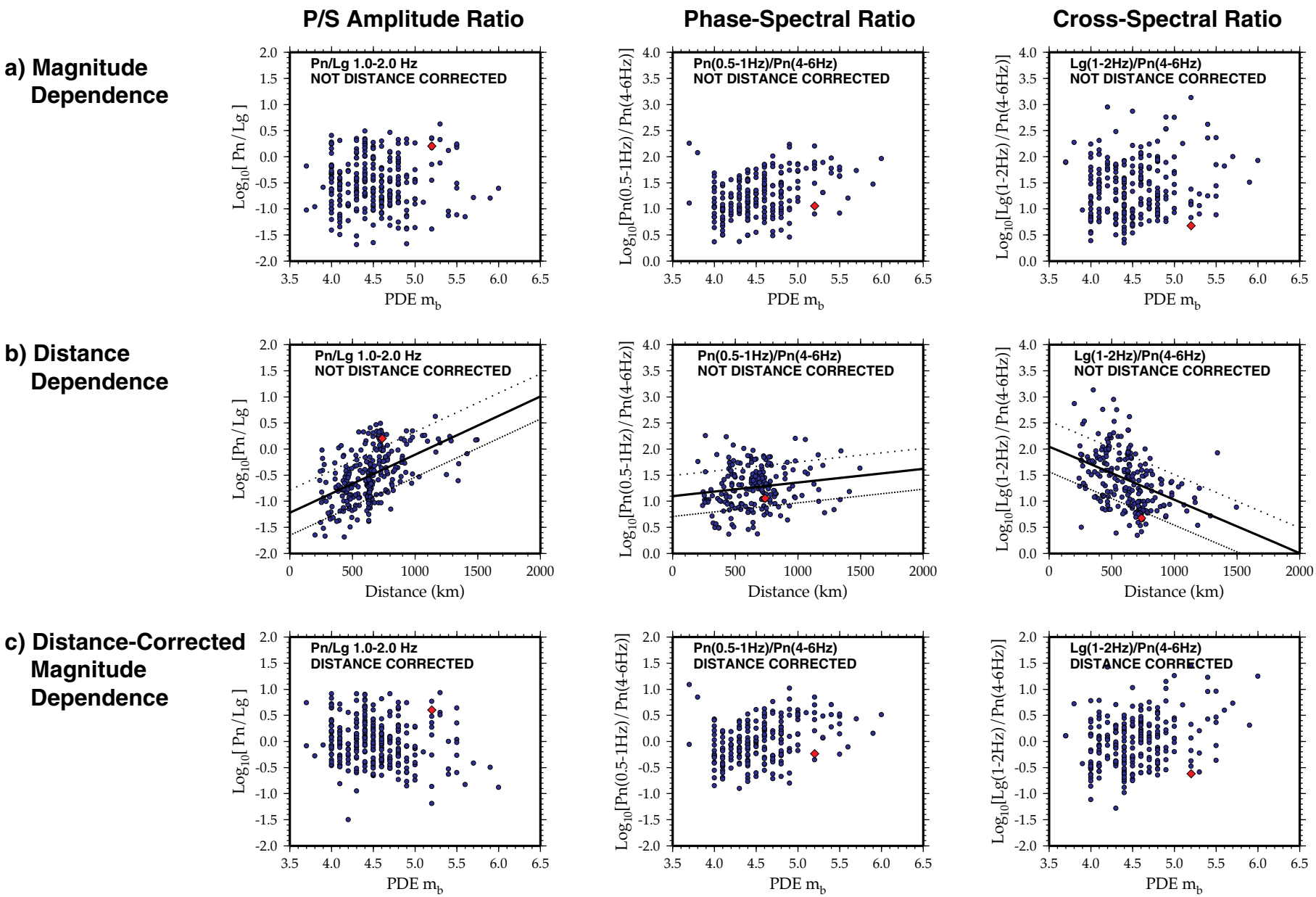

Rodgers and Walter, Regional Discrimination of Indian Test, 1999, Figure 3

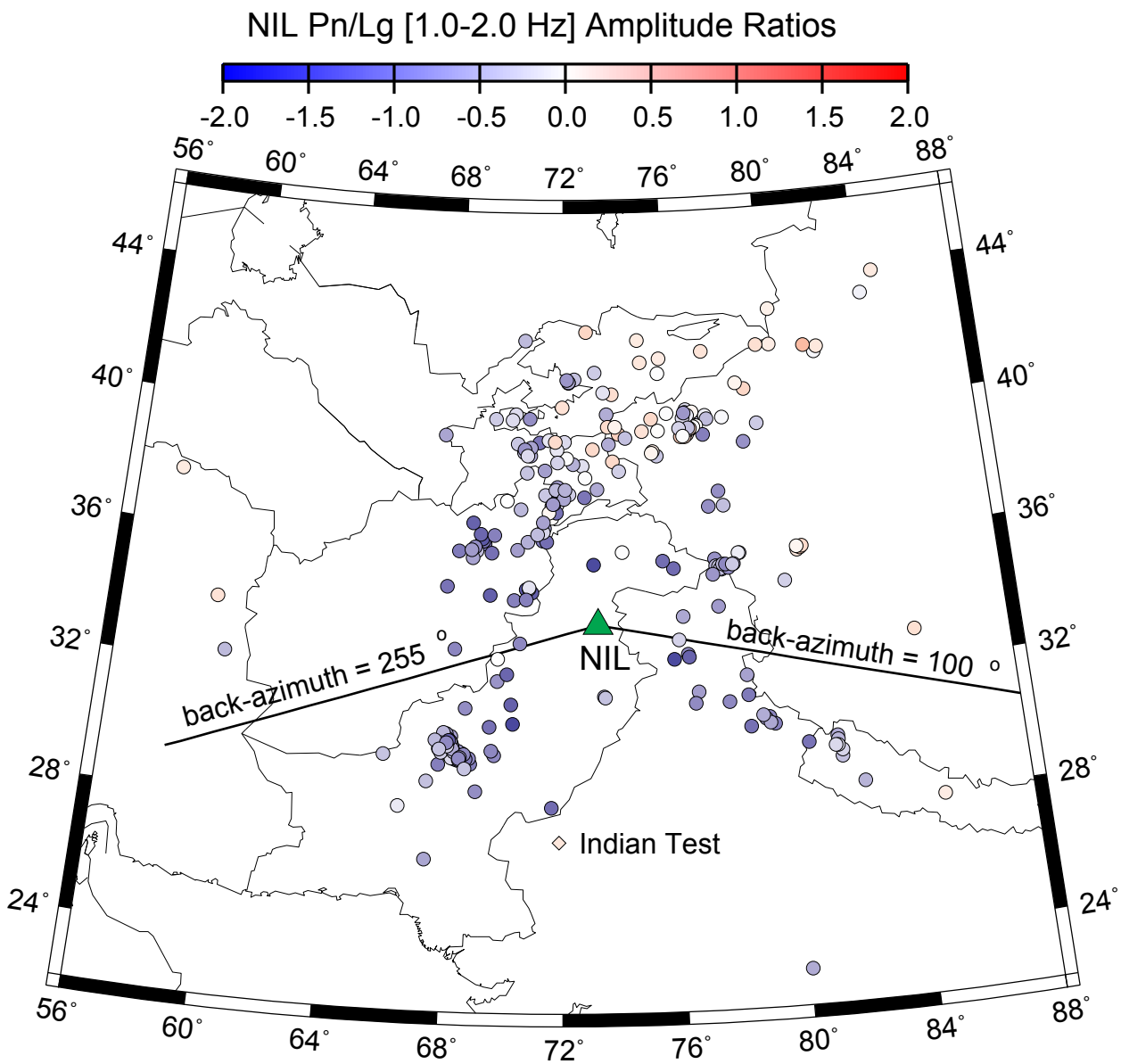

Rodgers and Walter, Regional Discrimination of Indian Test, 1999, Figure 4

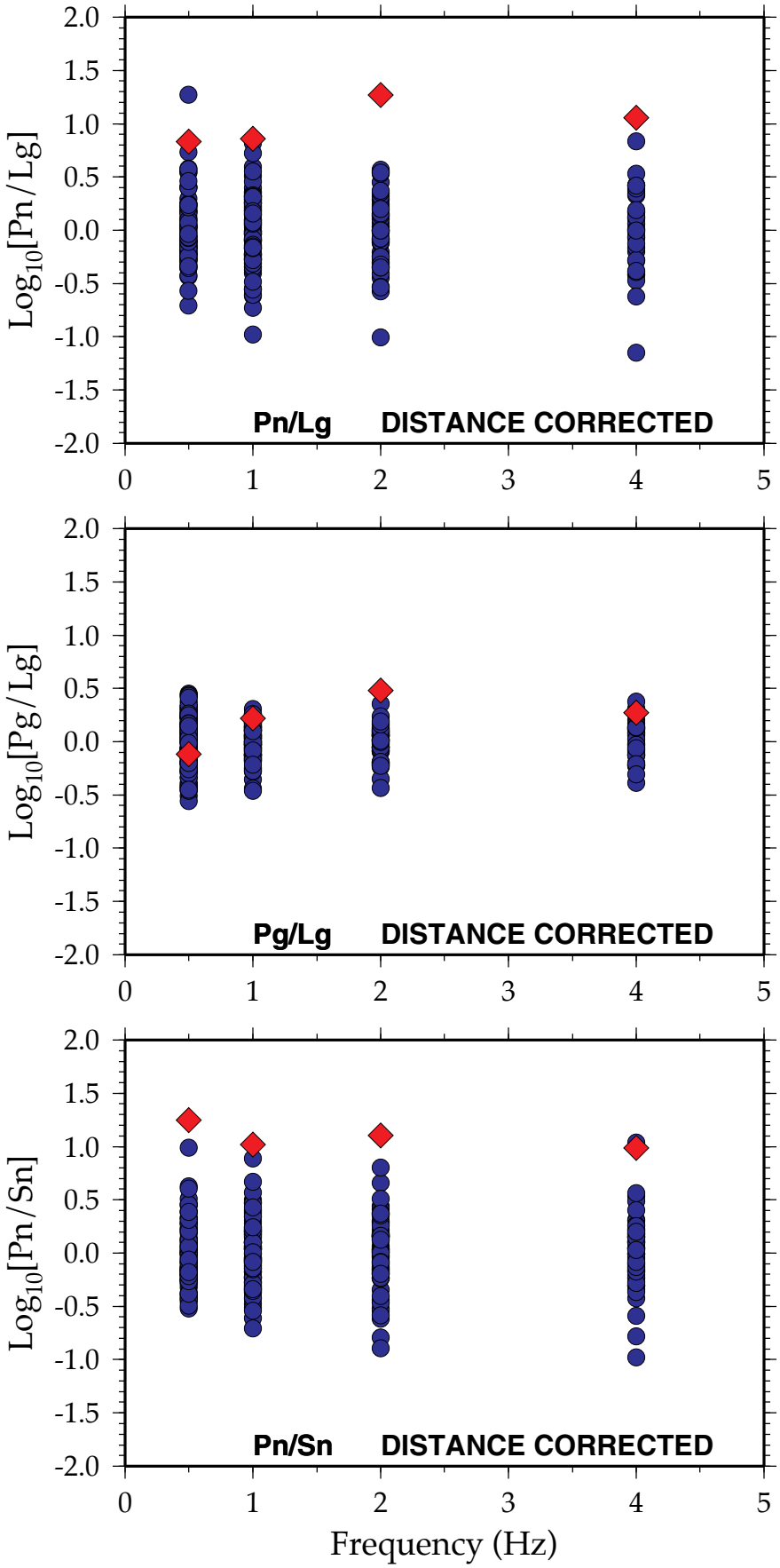

Rodgers and Walter, Regional Discrimination of Indian Test, 1999, Figure 5

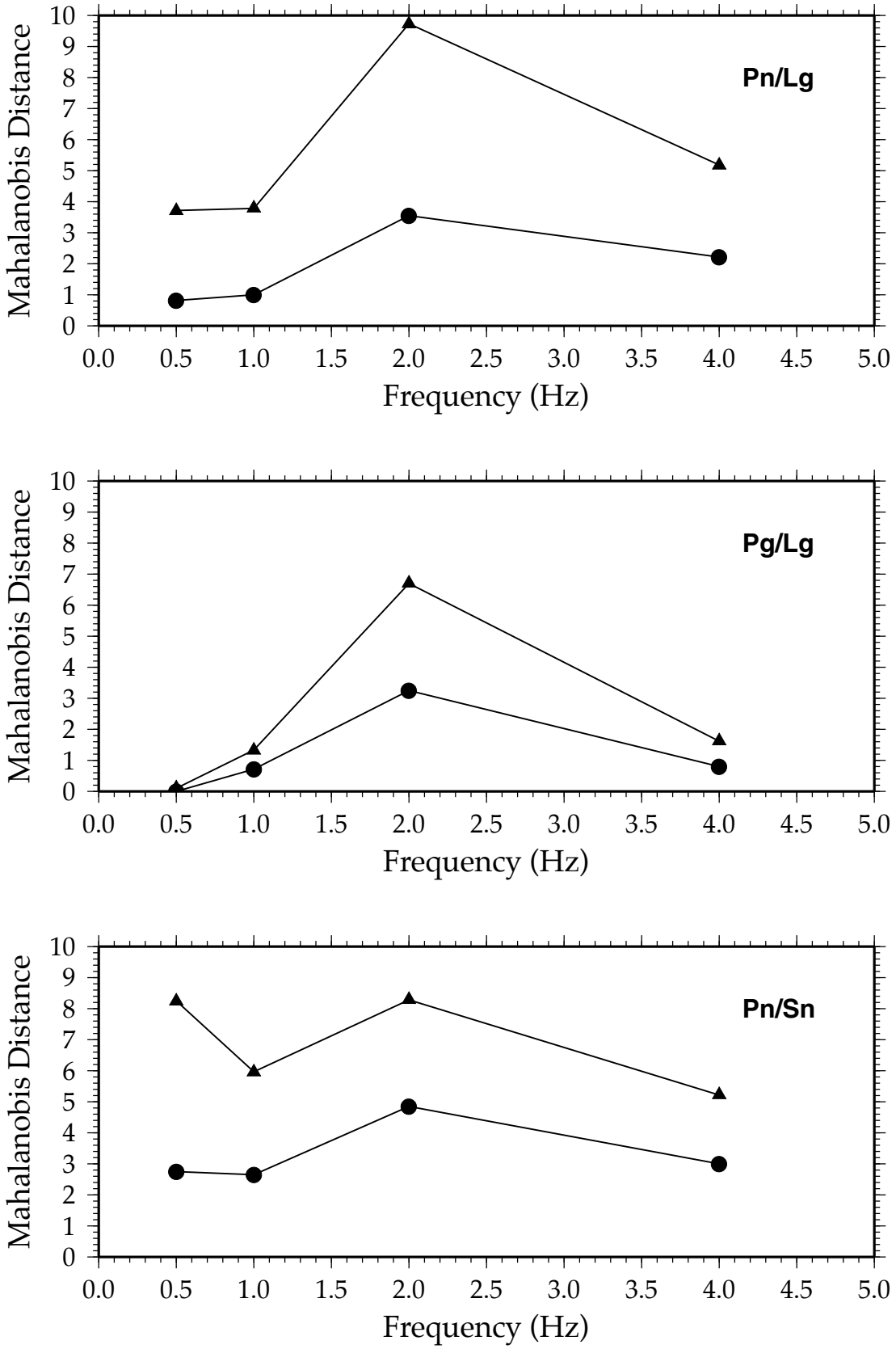

Rodgers and Walter, Regional Discrimination of Indian Test, 1999, Figure 6

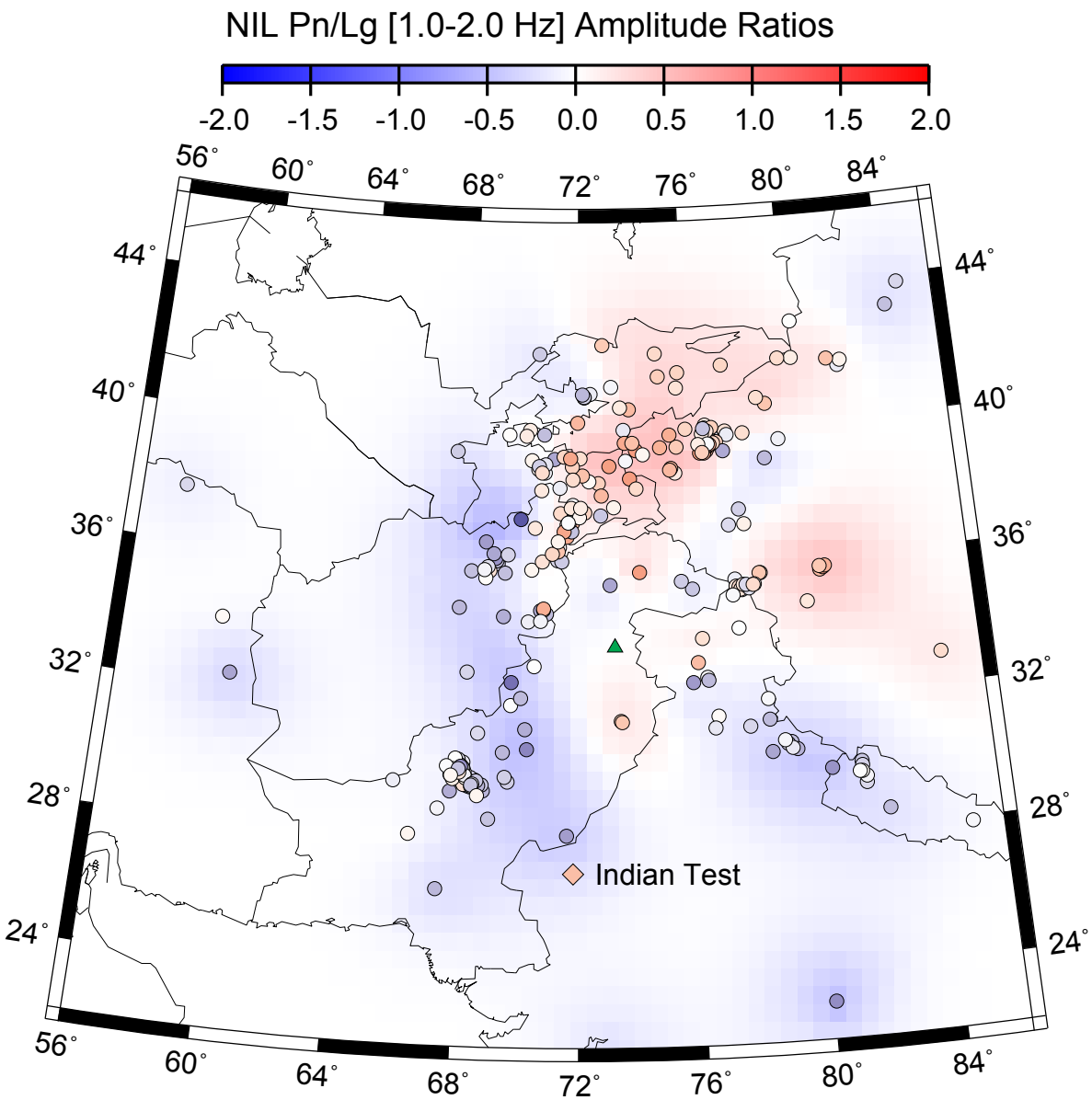

Rodgers and Walter, Regional Discrimination of Indian Test, 1999, Figure 7

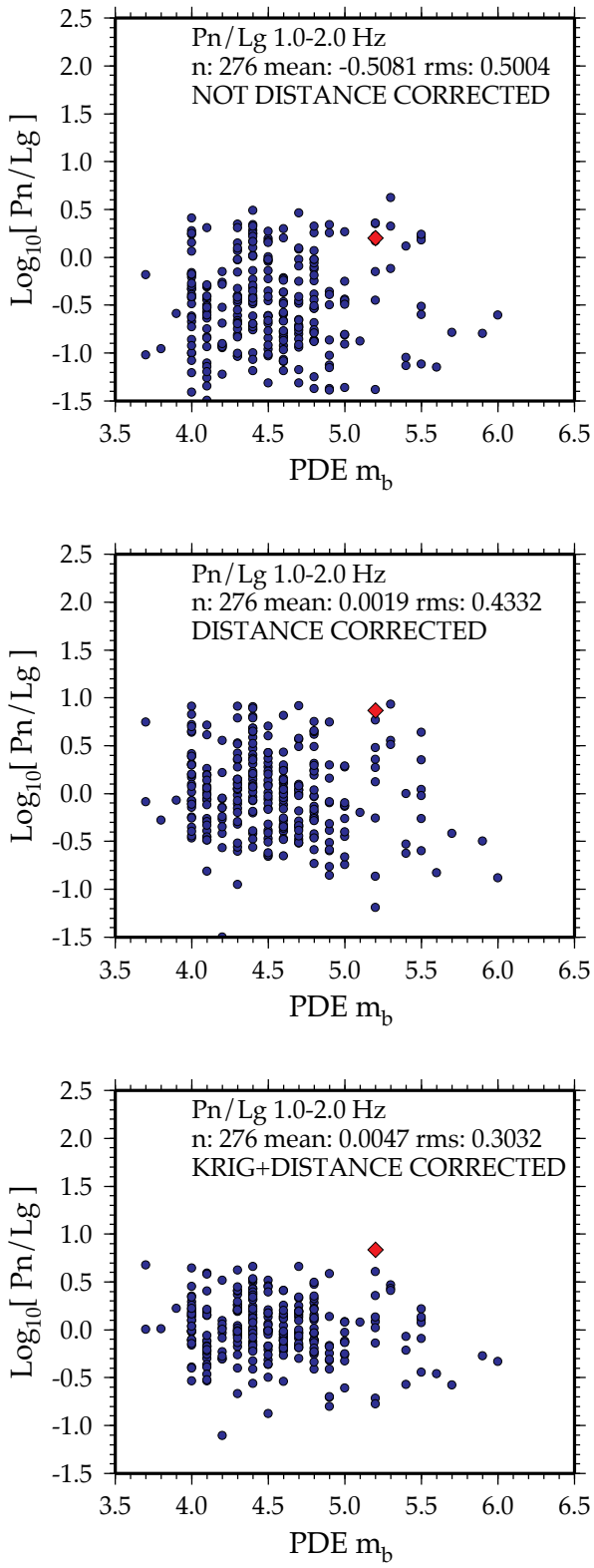

Rodgers and Walter, 1999, Regional Discrimination of Indian Test, Figure 8

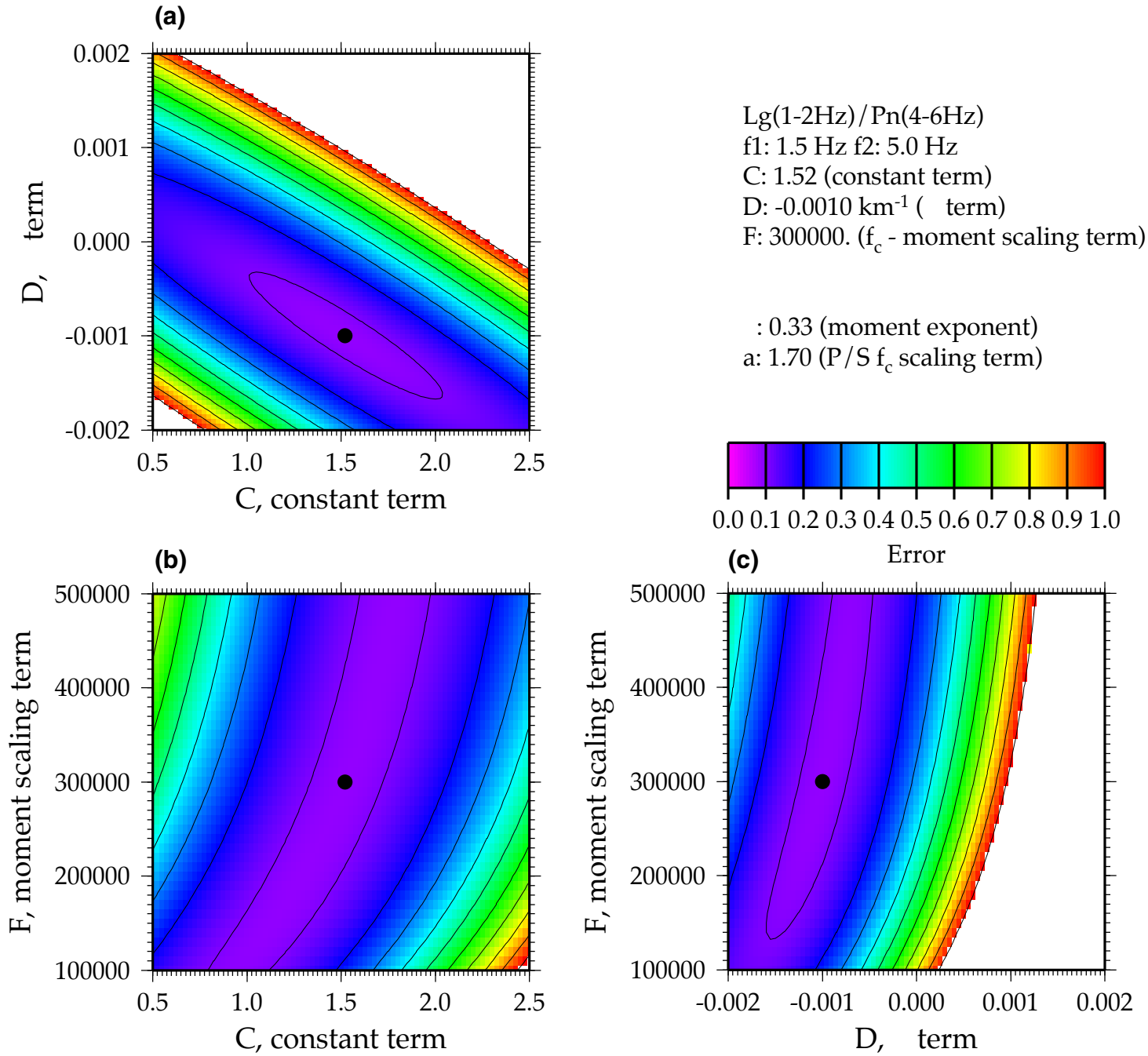

Rodgers and Walter, Regional Discrimination of Indian Test, 1998, Figure 9

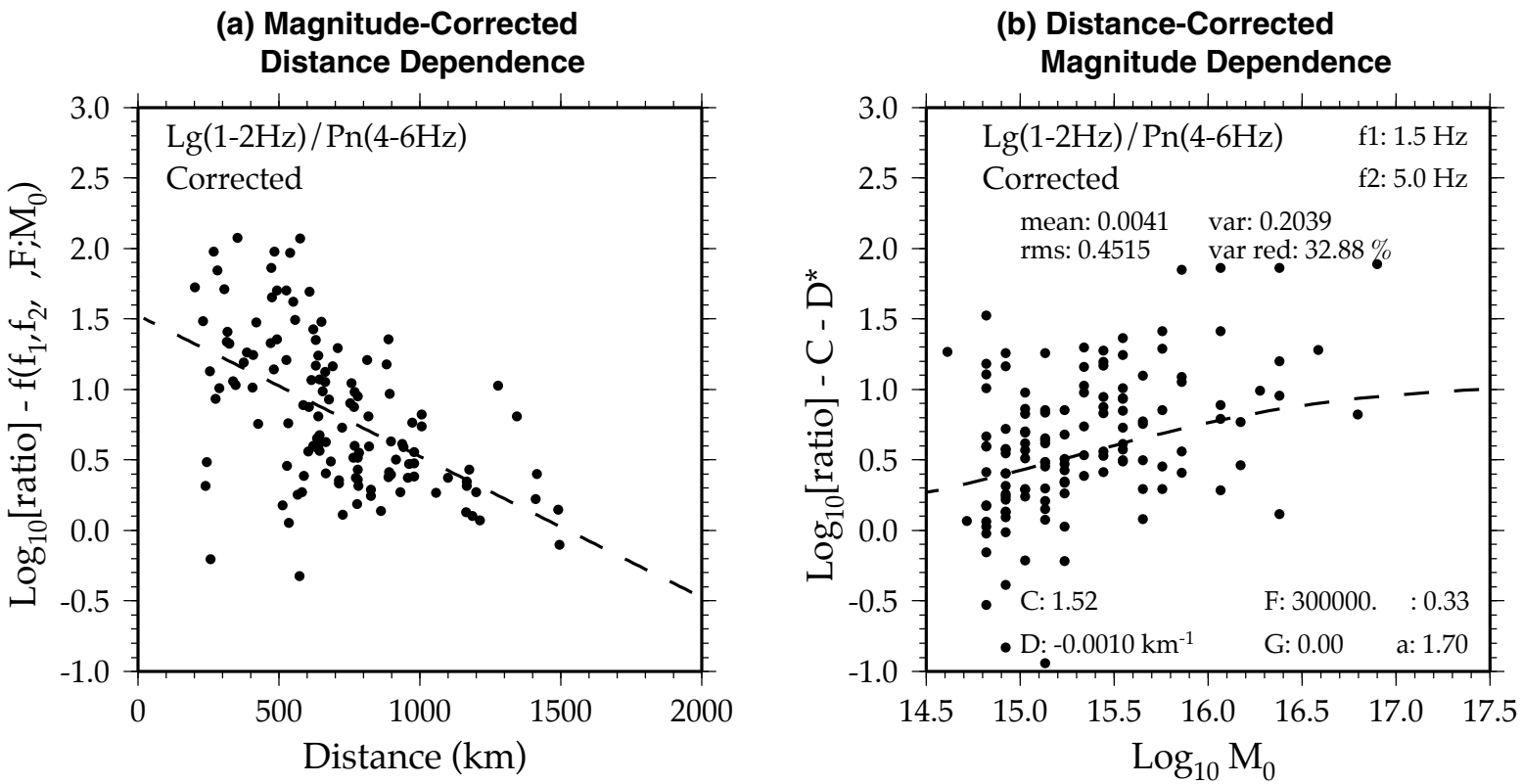

Rodgers and Walter, Regional Discrimination of Indian Test, 1998, Figure 10

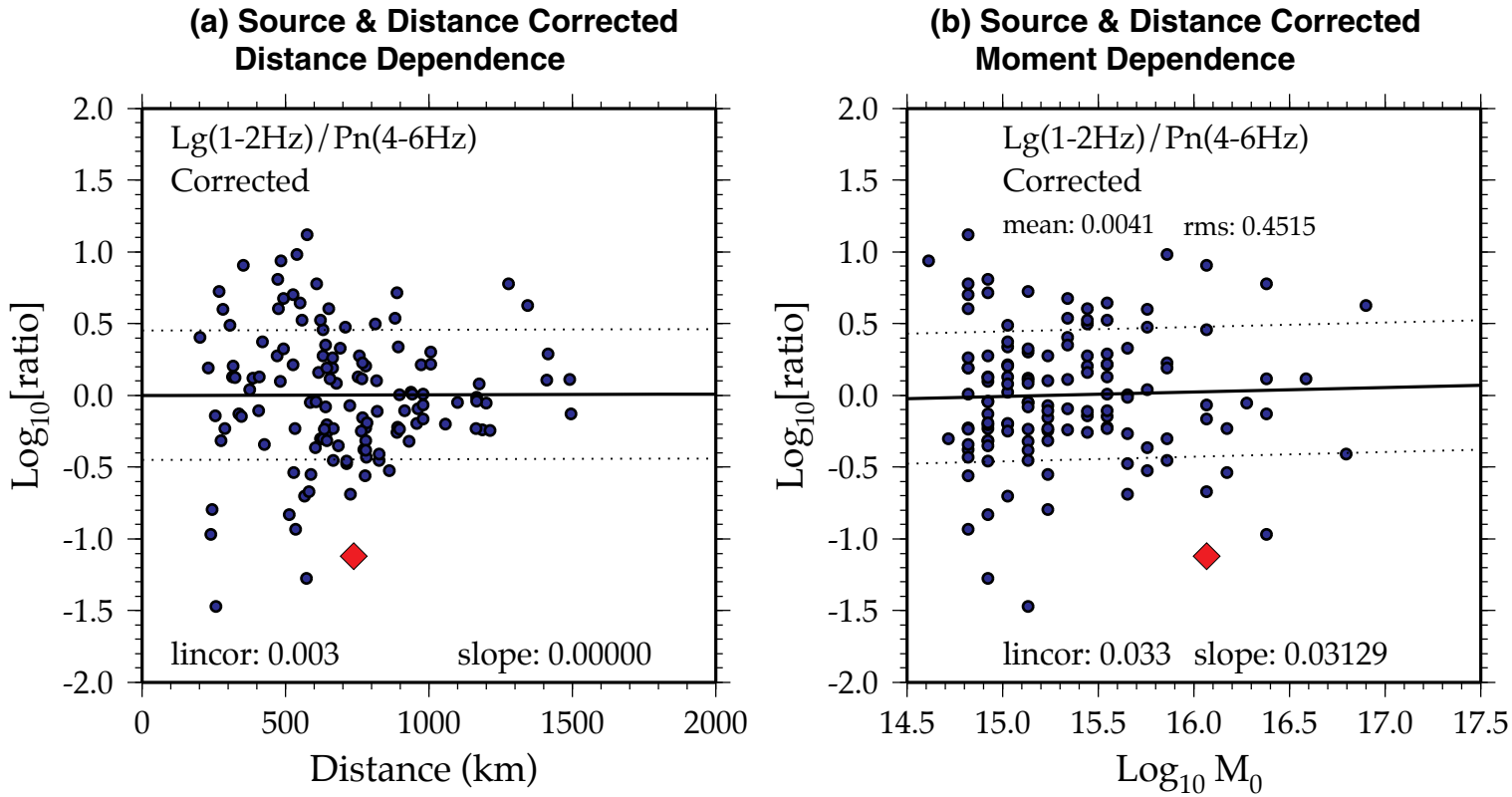

Rodgers and Walter, Regional Discrimination of Indian Test, 1998, Figure 11

Appendix - Magnitude and Distance Corrections for Spectral Ratios

Following Taylor and Hartse (1998), the amplitude spectrum of a short-period regional seismic phase (e.g. Pn, Pg, Sn, Lg), *A (f),* can be written as the product of three terms:

$$A(f) = S_0(f)\, G(\Delta)\, Q(f); \qquad (A1)$$

where f is frequency, Δ is distance, $S_0(f)$ is the source spectrum, $G(\Delta)$ is the (frequency independent) geometric spreading and $Q(f)$ is the attenuation operator. Note that a frequency dependent site effect can also be included in equation *(A1)*. We assume that the Brune (1970) model represents the source spectrum:

$$S_0(f) = c\, M_0 \left[1 - (f / f_c)^2 \right]^{-1} ; \qquad (A2)$$

where M_0 is the seismic moment, f_c is the corner frequency and c is a constant that depends on source and receiver material properties and the radiation pattern. The source corner frequency scales with the moment as:

$$f_c = F\, M_0^{-\kappa} ; \qquad (A3)$$

where F is the source moment corner frequency scaling parameter and κ is the source moment corner frequency scaling exponent. Examples of Brune model source spectra with the above corner frequency scaling are plotted in Figure A1a. The corner frequency of P- and S-waves can be different and related by:

$$f_c\,(P\text{-wave}) = a\, f_c\,(S\text{-wave}) \quad ; \qquad (A4)$$

where $1.0 \leq a \leq v_P/v_S \approx 1.7$. The geometric spreading is represented by the distance to a power:

$$G(\Delta) = \Delta^{-\gamma} ; \qquad (A5)$$

where γ is the geometric spreading exponent. The attenuation is represented as:

$$Q(f) = exp \left[- \omega t /2\, q(f) \right] = exp \left[- \pi f^{1-\eta} \Delta / U Q_0 \right] ;$$

(A6)

where $q(f) = Q_0 f^{\eta}$ is the frequency-dependent attenuation and U is the velocity of the phase in question.

Forming the S-wave to P-wave cross-spectral amplitude ratio, $S(f_1) / P(f_2)$, and ignoring the site effect and taking the base-10 log yields:

$$log_{10} [S(f_1) / P(f_2)] = - log_{10} \left[1 - (f_1 M_0^{-k} / a F)^2 \right] - \gamma^S log_{10} \Delta - \pi\, log10\, e\, f^{1-\eta S} \Delta / Q_{0S} U^S +$$

$$log_{10} \left[1 - (f_2 M_0^{-k} / F)^2 \right] + \gamma^P log_{10} \Delta + \pi\, log10\, e\, f^{1-\eta P} \Delta / Q_{0P} U^P;$$

(A7)

$$log_{10} [S(f_1) / P(f_2)] = log_{10} \left[1 - (f_2 M_0^{-k} / F)^2 \right] - log_{10} \left[1 - (f_1 M_0^{-k} / a F)^2 \right] +$$

$$\left[\gamma^P - \gamma^S \right] log_{10} \Delta + \pi\, log_{10}\, e \left[f_2^{1-\eta P} / Q_{0P} U^P - f_1^{1-\eta S} / Q_{0S} U^S \right] \Delta ; \qquad (A8)$$

where superscripts P and S identify P- and S-wave values. Note that the $log_{10} M_0$ term common to each amplitude cancels. We have assumed that radiation pattern effects are common to both phases. Strictly speaking this may not be true, however the effects of focal mechanism on short-period regional phase amplitudes is largely unknown. The site effects for each phase at the given frequencies, f_1 and f_2, lead to a constant term (independent of source moment and distance). Including the site effect constant, the above form *(A8)* can be represented as:

$$\log_{10} [S(f_1) / P(f_2)] = C + f(f_1, f_2, F, a, \kappa; M_0) + G \log_{10} \Delta + D \Delta \; ; \qquad \text{(A9)}$$

where

$$f(f_1, f_2, F, a, \kappa; M_0) = \log_{10} \left[1 - (f_2 M_0^{-k} / F)^2 \right] - \log_{10} \left[1 - (f_1 M_0^{-k} / a F)^2 \right] . \qquad \text{(A10)}$$

The function $f(f_1, f_2, F, a, \kappa; M_0)$ is plotted in Figure A1b for the Lg[1-2 Hz]/Pn[4-6 Hz] spectral ratios modeled in the text. The term D can be related to the attenuation parameters Q_0 , η and U for P- and S-waves. The term G is identically equal to $[\gamma^P - \gamma^S]$. We have not found this term to be resolvable from the linear distance term, D, probably because scatter in the data from path propagation effects out weighs the effects of the log-distance term.

There are two distinct advantages of this method. Firstly, we only need to specify two parameters (κ and a) and search for three parameters (C, D and F). And secondly, the dependence of the spectral ratios on distance and magnitude (log moment) can be completely removed.

Figure Caption

Figure A1. (a) Examples of Brune model source spectra using the source moment-corner frequency scaling parameters: κ = 1/3, a = 1.7 and F = 300000. Spectra are shown for various moments with moment magnitudes, M_W, identifying each curve. (b) Moment dependence of spectral ratios specified by the function $f(f_1, f_2, F, a, \kappa; M_0)$ using the best-fitting parameters from our gridsearch modeling for the Lg [1-2 Hz] / Pn [4-6 Hz] ratios.

(a)

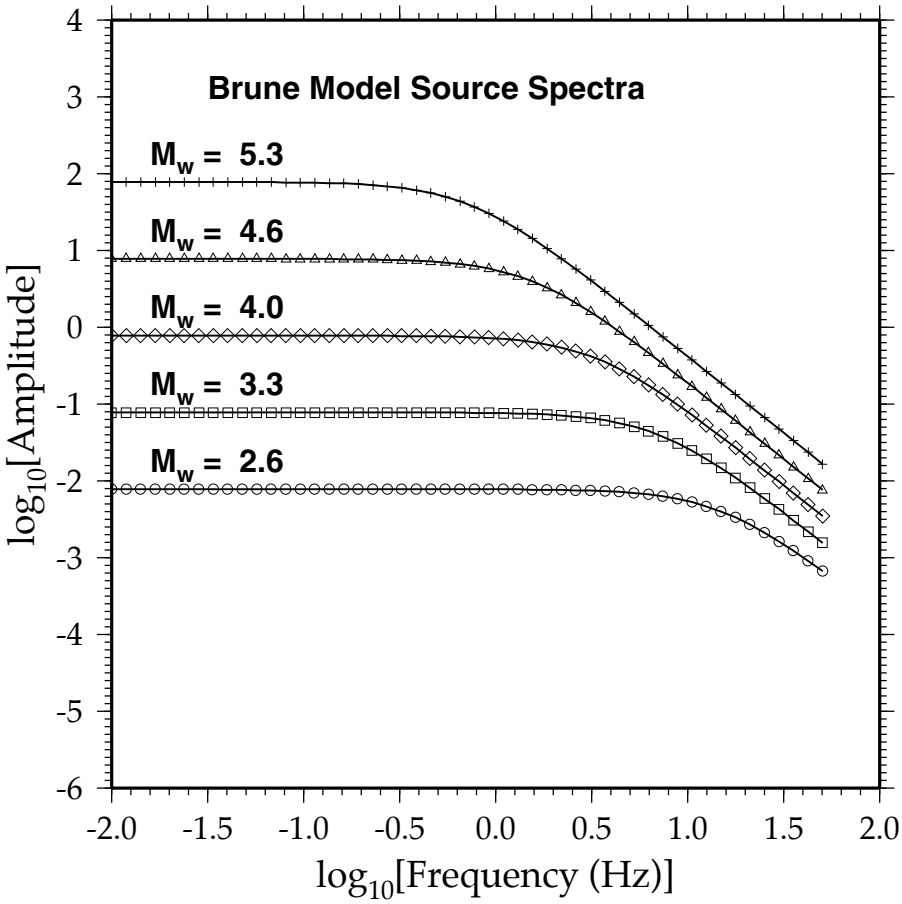

(b)

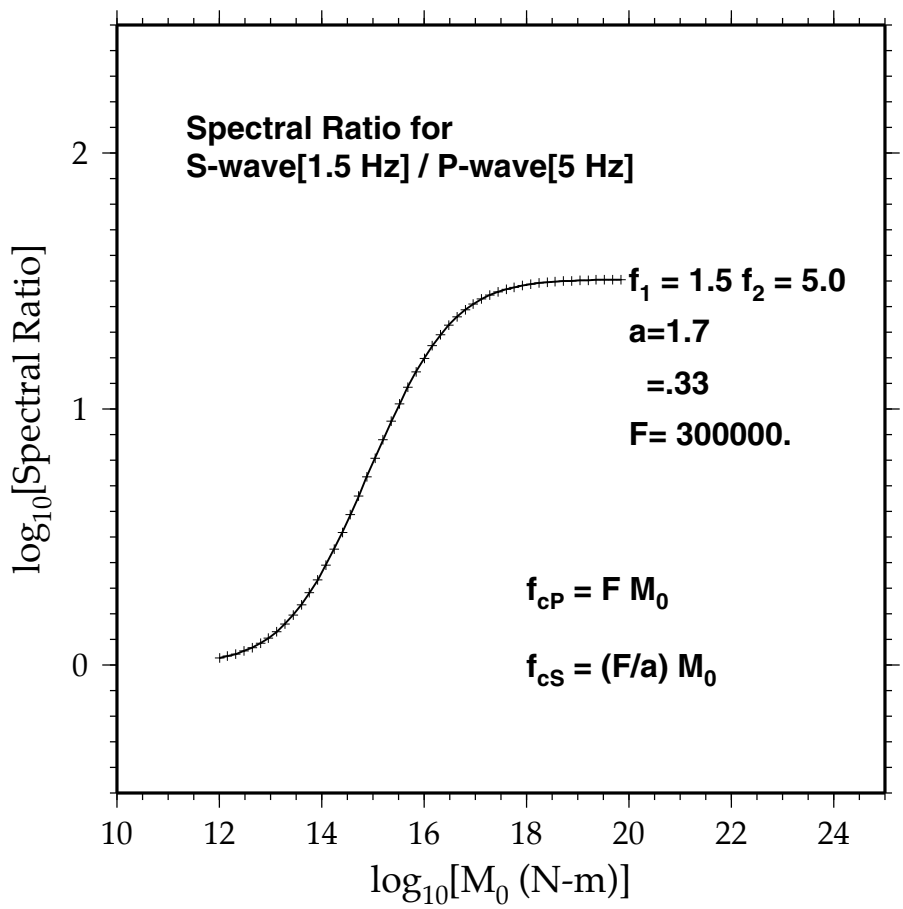

Rodgers and Walter, Regional Discrimination of Indian Test, 1998, Figure A1